Experimental Phase Diagram of Perpendicularly Magnetized Ultrathin Ferromagnetic Films

N. Saratz, A. Lichtenberger, O. Portmann, U. Ramsperger, A. Vindigni, and D. Pescia
Laboratory for Solid State Physics, ETH Zurich, 8093 Zurich, Switzerland
(Received 18 November 2009; published 19 February 2010)

We image the domain patterns in perpendicularly magnetized ultrathin Fe films on Cu(100) as a function of the temperature T and the applied magnetic field H. Between the low-field stripe phase and the high-field uniform phase we find a bubble phase, consisting of reversed circular domains in a homogeneous background. The curvature of the transition lines in the $H - T$ parameter space is in contrast to the general expectations. The pattern transformations show yet undetected scaling properties.

DOI: 10.1103/PhysRevLett.104.077203 PACS numbers: 75.70.Kw, 05.70.Fh, 75.30.Kz, 75.70.Ak

Domain patterns form spontaneously in a wide variety of physical or chemical systems, ranging from type I superconductors in the mixed state [1] to diblock copolymers [2], thermal convection [3] or monolayers of amphiphilic molecules at the air-water interface [4]. The common phenomenology in these microscopically very different systems can be explained if the pattern is viewed as a modulated phase [5]. Modulation generally results if a short-ranged attractive interaction, favoring a uniform ordered state, is frustrated by a weaker, but long-ranged, repulsive interaction. The modulated order parameter may represent quantities as diverse as the spin density, the charge density in any type of strongly correlated classical or quantum system [6], the volume fraction of diblock copolymers, the concentration of amphiphilic molecules and other chemical species, or dipolar bosons in an optical lattice [7]. Most common patterns in two-dimensional systems include regular arrays of stripes or circular bubbles. The actual pattern realized in a given system depends on parameters such as temperature, the volume fraction of the constituents or external fields. A mean-field phase diagram of systems with modulation along two dimensions has been computed by Garel and Doniach [8] for micrometer-thick magnetic garnet films, considering stripe-, bubble- and uniform phases. This phase diagram is widely accepted as the generic phase diagram for two-dimensional modulated systems [5,9], although for ultrathin magnetic films a topologically different phase diagram has been predicted, considering stripe- and uniform phases only [10]. In spite of the large scientific effort on many different systems, *experimental* confirmation of any of these phase diagrams is, to our knowledge, still missing.

In this Letter we image the magnetic domain patterns in perpendicularly magnetized Fe films on Cu(100) as a function of the temperature and the externally applied magnetic field. We find that in a restricted region of temperatures the transitions between the different domain patterns occur in thermal equilibrium and determine the transition lines dividing the stripe- from the bubble- and the uniform phases. While the appearance of these three phases is in agreement with Ref. [8], the curvature of the transition lines is in qualitative agreement with the phase diagram proposed in Ref. [10] and thus at odds with the general expectation [5,9]. The experimental data reveal scaling aspects which have remained undetected yet.

The system we investigate in this Letter consists of ≈ 2 atomic layers of Fe grown epitaxially on a Cu(100) single crystal surface [11–13]. The Fe spins are grouped into magnetic domains with spins pointing parallel or antiparallel to the film normal. The origin of the magnetic domains is the competition between the short-ranged exchange interaction favoring parallel alignment of neighboring spins and the much weaker but long-ranged dipolar interaction favoring antiparallel alignment. An applied magnetic field establishes a preferred spin orientation. Imaging of the spatial spin distribution at variable applied magnetic fields and variable temperature is performed by scanning electron microscopy with polarization analysis (SEMPA) with a lateral resolution of 50 nm [13,14]. In the images, the perpendicular component of the magnetization is displayed as a gray scale.

Figures 1(a)–1(e) [13] show the typical sequence of domain patterns while the sample is continuously cooled in a constant applied field. At high temperature, Fig. 1(a), we observe a state with uniform spin distribution, the u state. Upon cooling, a transition leads to a striped domain configuration, the s state; Figs. 1(b) and 1(c). As the sample is cooled further, the s state transforms into a bubble phase (the b state, Figs. 1(d) and 1(e) [15]). Additional cooling produces a third transition, $b \rightarrow u$, Fig. 1(e), at which a uniform magnetization of the sample is reached. Upon heating the film from the low-temperature uniform state, we observe the reverse sequence $u \rightarrow b \rightarrow s \rightarrow u$ (not shown). By imaging at constant temperature while increasing the magnetic field, Figs. 1(f)–1(j), we observe the sequence $s \rightarrow b \rightarrow u$ [16].

Repeating the imaging process along different paths in the $T - H$-parameter space allows measuring the phase-transition lines $H_{s\rightarrow b}(T)$, solid symbols in Fig. 2(a), and $H_{b\rightarrow u}(T)$, open symbols in Fig. 2(a). The circles correspond to measurements at constant magnetic field as in Figs. 1(a)–1(e), triangles represent measurements at con-

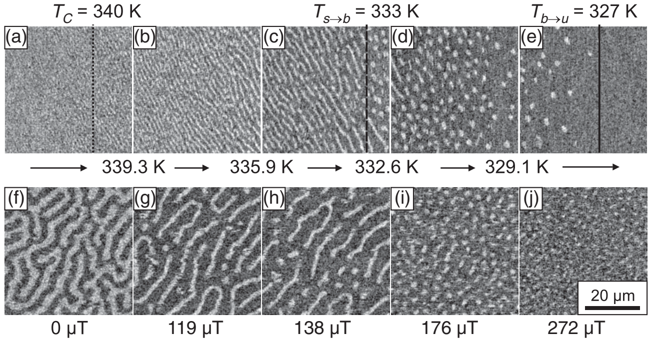

FIG. 1. Sequence of magnetic domain patterns. Images (a) to (e) are obtained by cooling the sample at a constant rate of -0.5 K/min in a constant field of 146 μT. During the measurement of each image the temperature changes by 3.5 K, with different positions corresponding to different temperatures. The temperature values between the images are indicated. The pattern evolves from uniform (a) to stripes (b)–(c) to bubbles (d)–(e) to uniform (e), the transition temperatures are indicated by the vertical lines. Images (f) to (j) are recorded at a constant temperature of 350 K ($T/T_C = 0.99$) and the field is increased stepwise between the images. The observed sequence is stripes (f) to bubbles (i)–(j) to uniform (not shown). The applied field is indicated for each image. The series (a)–(e) and (f)–(j) have been measured on two different samples.

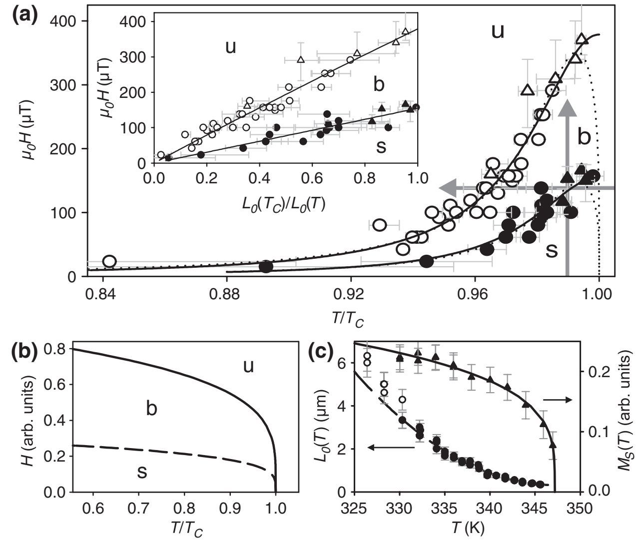

FIG. 2. Phase diagram and scaling of the transition fields. (a) Experimental phase diagram in $T-H$ space. The transition points obtained in constant field (circles) and at constant temperature (triangles) are shown for the transitions stripes $\to$ bubbles (solid symbols) and bubbles $\to$ uniform (open symbols). The gray arrows indicate the paths followed for the measurement of Fig. 1. The solid and dotted lines indicate fits to the transition lines using $1/L_0(T)$ and $M_S(T)/L_0(T)$ scaling, respectively, where $L_0(T)$ is the stripe width in zero field and $M_S(T)$ the local magnetization inside the domains [13]. The error bars indicate the upper and lower bounds for the transitions as determined from visual inspection of the SEMPA images. The scaled phase diagram (inset) demonstrates the $1/L_0(T)$ scaling of the transition fields. The solid lines are the same as in (a). (b) Standard phase diagram for modulated systems for comparison, adapted from Ref. [8]. (c) Experimental behavior of $M_S(T)$ (triangles, right scale) and $L_0(T)$ (circles, left scale). The lines are fits to the solid symbols using power laws $M_S(T) = M_\beta(1 - T/T_C)^\beta$ with $\beta \approx 0.25$ and $L_0(T) = L_0(T_C) + L_1(1 - T/T_C)^2$ [12]. The local magnetization $M_S(T)$ varies only weakly over most of the temperature range and rapidly drops to zero close to T_C. In contrast, $L_0(T)$ decreases strongly with increasing temperature, reaching a finite value $L_0(T_C)$ as T approaches T_C.

stant temperature as in Figs. 1(f)–1(j). The phase-transition lines are curved *upward* over most of the temperature range. This result is in contrast to the phase diagram of Ref. [8] reproduced schematically in Fig. 2(b): In Fig. 2(b), the pattern sequence when decreasing the temperature at constant applied field is $u \to b \to s$, while it is $(u \to)s \to b \to u$ in the present experiments. Figure 2(c) shows the temperature dependence of two important experimental quantities: the local magnetization inside the domains ($M_S(T)$ [13], triangles) and the domain size in zero field ($L_0(T)$ [13], circles). In zero field, we can identify a transition temperature T_C [13] at which $M_S(T)$ vanishes and with it the contrast in the SEMPA images. Because of the vanishing contrast, we are only able to image the domain patterns reliably up to $\approx$1 K below T_C. In the inset of Fig. 2(a), we use the experimental $L_0(T)$ of Fig. 2(c) to replot the phase-transition lines using the variable H along the vertical axis and the variable $\frac{L_0(T_C)}{L_0(T)}$ along the horizontal axis. The observed linear behavior [the straight lines in the inset are equivalent to the solid lines through the data points in Fig. 2(a)] establishes a first scaling law, namely, that the critical fields $H_{s\to b}(T)$ and $H_{b\to u}(T)$ scale with $\frac{1}{L_0(T)}$. This scaling law relates the upward bending of the transition lines to the strong decrease of L_0 with T. Note that the ratio $\frac{H_{s\to b}(T)}{H_{b\to u}(T)} \approx 0.41$ is independent of temperature (or, equivalently, of L_0).

For a more quantitative description of the transition, we introduce the pattern asymmetry $A(T, H) \doteq \frac{f_\uparrow - f_\downarrow}{f_\uparrow + f_\downarrow}$, $f_{\uparrow(\downarrow)}$ being the area within an image occupied by up ($\uparrow$) or down ($\downarrow$) spins [13]. In Fig. 3(a), a family of $A(T, H = \text{const})$ curves for different values of H is shown. Note that the open triangles identifying $T_{s\to b}$ are located within a horizontal band [gray in Fig. 3(a)], which suggests that the value of A at the $s \to b$ transition, $A_{s\to b} = 0.436 \pm 0.022$, is independent of temperature. In contrast, when increasing the field at constant temperature, Fig. 3(b), for low T a metastable stripe phase is often observed to persist up to higher fields and higher values of A than expected from the measurements in constant field. This is due to the fact that the main process leading from stripes to bubbles at constant T is stripe fission, which is less efficient at lower temperatures. Figure 3(c) shows that $A_{s\to b}$ obtained at constant T corresponds to the equilibrium value (gray bands) only close to T_C and tends to increase for decreas-

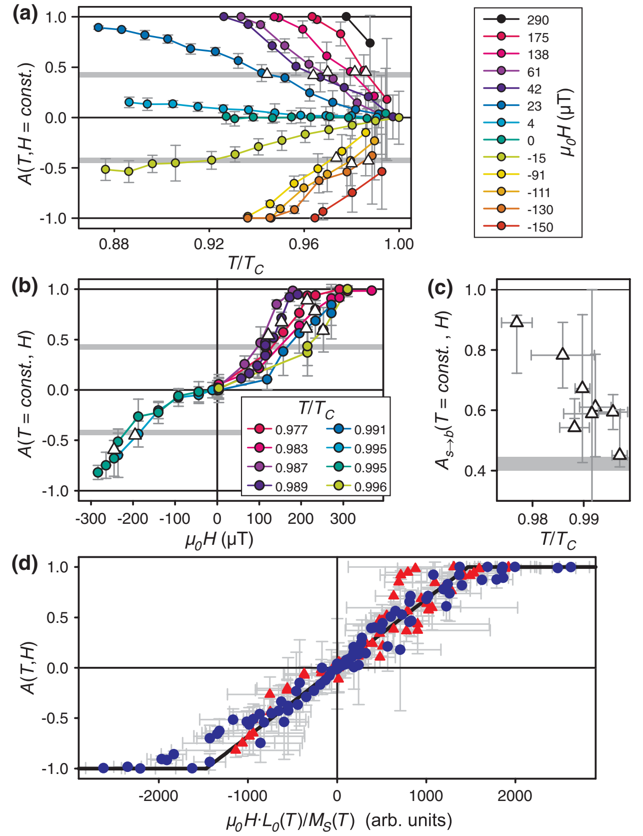

FIG. 3 (color online). (a) Pattern asymmetry $A(T, H = \text{const})$ observed upon cooling in constant field. The field value in μT is indicated in the legend for every curve connecting the $A(T, H)$ data points obtained from individual images within a series (circles). Empty triangles indicate $T_{s\to b}$ for each series, the gray bars indicate the calculated ground-state transition interval. (b) Pattern asymmetry $A(T = \text{const}, H)$ upon increasing the field at constant temperature. The reduced temperatures T/T_C are indicated in the legend. (c) Pattern asymmetry at the $s \to b$-transition ($A_{s\to b}$) from Fig. 3(b) vs reduced temperature. (d) Collapse plot of the asymmetry values $A(T, H = \text{const})$ (blue circles) and $A(T = \text{const}, H)$ (red triangles) of the individual images from figures (a) and (b). Some measurements shown in (d) are not shown in (b) for better clarity. The solid line is a guide to the eye.

ing values of the constant temperature. The domain pattern may thus depend on the (T, H) history of the sample at low T, as is also the case for the -15 μT curve of Fig. 3(a), where the $s \to b$ transition is suppressed. However, within its error, the asymmetry $A(T, H)$ is a well-defined function in the entire temperature range investigated here, irrespectively of the actual pattern that is realized. Moreover, plotting $A(T, H)$ vs $H\frac{L_0(T)}{M_S(T)}$ produces a collapse of all data points onto one single scaling function, Fig. 3(d), which establishes a second scaling law.

The two empirical scaling laws are also observed in ground-state calculations, where L_0 is varied not by changing the temperature but by changing the relative strength of the two competing interactions. The total energy in the ground state is computed by minimizing the total energy of a slab of variable thickness d along the z direction and lateral size $\Lambda \gg d$ in the x-y plane [13]. With the field H applied along the $+z$ direction we consider the following patterns: alternating stripes (s) of width $L \pm \delta$ and magnetization $\pm M_S$, a hexagonal array of reversed ($m = -M_S$) bubbles (b) of radius R and center spacing L_B in a homogeneous background ($m = +M_S$) and the uniform (u) state ($m = +M_S$). For each value of H, the total energy of each pattern is minimized with respect to L and δ or R and L_B respectively. In zero field, stripes of alternating magnetization $\pm M_S$ and equal width $L = L_0$ are energetically favored [17]. By comparing the energies of the s, b and u states, we obtain the ground-state phase diagrams Fig. 4(a) and 4(b), where the transition fields $H_{s\to b}$, $H_{b\to u}$ and $H^*_{b\to u}$ are plotted for (ultra-)thin films with $d \ll L_0$ [Fig. 4(a)] and thick films with $d \gg L_0$ [Fig. 4(b)]. For thin films, we find numerically (and partly analytically) that the transition fields H_t obey the scaling law $H_t/M_S \propto 1/L_0$ [Fig. 4(a)]. If we assume the same scaling law to hold for our experiments at finite temperatures, we obtain the dotted lines in Fig. 2(a). From our data it is not possible to discriminate between the two scaling laws $H_t(T) \propto M_S(T)/L_0(T)$ [dotted lines in Fig. 2(a)] and $H_t(T) \propto 1/L_0(T)$ [solid lines in Fig. 2(a)]: At intermediate T the

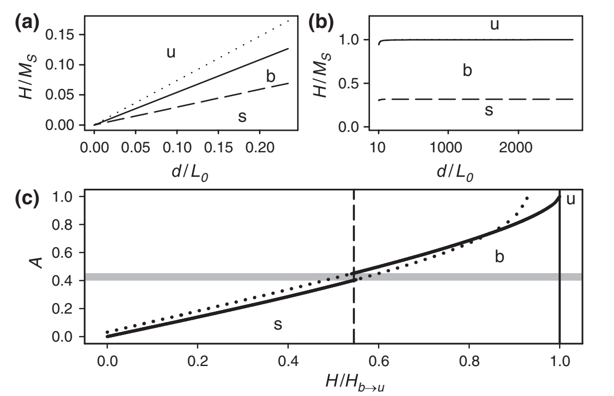

FIG. 4. Ground-state calculations. (a) Theoretical ground-state phase diagram in $H/M_S - 1/L_0$-space for thin and (b) thick films. The dashed lines mark $H_{s\to b}$. At the critical field $H_{b\to u}$ (solid line), the energy of the bubble lattice equals the energy of the uniform state. In a range of fields above $H_{b\to u}$, however, a state with isolated bubbles is still a local minimum of the energy. Above the critical field $H^*_{b\to u}$ (dotted line) this local energy minimum disappears. In (b), $H_{b\to u} \approx H^*_{b\to u} \approx M_S$. (c) Ground-state behavior of the pattern asymmetry $A(H)$ for the case $d \ll L_0$. The solid curve represents $A(H)$ for the equilibrium pattern, i. e. stripes at low fields and bubbles at high fields. The dotted lines continue $A(H)$ for both patterns to the field ranges where they are metastable, i.e., to low fields for bubbles and to high fields for stripes. The vertical lines mark the equilibrium transitions from stripes to bubbles (dashed) and from bubbles to uniform (solid). The gray bar indicates the discontinuity in $A(H)$ at the equilibrium transition from stripes to bubbles.

temperature dependence of $H_t(T)$ is dominated by the strong temperature dependence of $L_0(T)$ [Fig. 2(c)], and in the immediate proximity to T_C, where the dotted lines suggest a downward-bending of the transition lines, imaging of the domain patterns is not feasible as pointed out before [12]. Therefore, in our experiments we cannot resolve the phase-transition lines in this region.

Nevertheless, the agreement between the experimentally observed scaling laws and the ones inferred from the ground-state computations suggests that the experimental phase diagram at finite temperatures can be obtained—at least qualitatively—by assuming the ground-state phase diagram and substituting M_S with $M_S(T)$ and L_0 with $L_0(T)$.

In the present system, the strong temperature dependence of $L_0(T)$ [18] outweighs the effect of the decreasing magnetization $M_S(T)$ [Fig. 2(c)] and the transition lines are curved upward as discussed for Fig. 2(a), in qualitative agreement with Ref. [10]. For thick films instead, the ground-state results suggest $H_t \propto M_S$ and—most important—H_t independent of L_0, so that we can obtain the finite temperature transition lines of Fig. 2(b) by simply assuming the ground-state phase diagram and substituting in it M_S with $M_S(T)$. Accordingly, for thick films with $d \gg L_0$ [5,8,19], the transition fields are proportional to M_S and their temperature dependence is ruled by $M_S(T)$, resulting in down-bent transition lines as in Fig. 2(b), in agreement with Ref. [8].

Figure 4(c) shows the numerically computed $A(H)$ in the ground state for the case $d < L_0$ for stripe- and bubble patterns. For both patterns it is found to vary almost linearly with $H/H_{b\rightarrow u}$, apart from a nonanalytic behavior in the close proximity of $H_{b\rightarrow u}$, and $A(H)$ is rather insensitive to the geometry of the domain pattern. The transition from stripes to bubbles at $H_{s\rightarrow b}$ leads to a small discontinuity in the equilibrium $A(H)$ (solid line). By combining this linear behavior with the fact that $H_{b\rightarrow u} \propto M_S/L_0$ we can write down the approximate ground-state scaling law $A(H) \propto H(L_0/M_S)$. Again, the same scaling law as observed experimentally close to T_C in Fig. 3(d). Note that in the ground state the $s \rightarrow b$ transition is found for $A_{s\rightarrow b} \in [0.402, 0.454]$ [gray bar in Fig. 4(c) [20]], the same number we observe experimentally close to T_C (gray bars in Figs. 3(a)–3(c). In addition, the ground-state ratio $\frac{H_{s\rightarrow b}}{H^*_{b\rightarrow u}} = 0.401$ coincides with the experimental ratio measured at finite temperatures.

In summary, the discovery in Ref. [15] of a bubble phase in ultrathin magnetic films inspired us to search for an experimental proof of the equilibrium phase diagram proposed originally in 1982 by Garel and Doniach [8]. We have found that the phase-transition lines [Fig. 2(a)] are in qualitative agreement with Ref. [10] and we have provided some arguments suggesting that the difference between the two phase diagrams is due to the different thickness regimes. The observation of scaling laws and characteristic constants which appear to be valid at all temperatures suggests the existence of some kind of underlying scaling invariance which appears to have escaped detection so far in theoretical (and experimental) work on modulated systems.

We thank Thomas Bähler for technical assistance as well as the Swiss National Science Foundation and ETH Zurich for financial support.

[1] R. Prozorov, A. F. Fidler, J. R. Hoberg, and P. C. Canfield, Nature Phys. **4**, 327 (2008).
[2] F. S. Bates, Science **251**, 898 (1991).
[3] E. Bodenschatz, J. R. de Bruyn, G. Ahlers, and D. S. Cannell, Phys. Rev. Lett. **67**, 3078 (1991).
[4] D. Andelman, F. Brochard, and J.-F. Joanny, J. Chem. Phys. **86**, 3673 (1987).
[5] M. Seul and D. Andelman, Science **267**, 476 (1995).
[6] C. B. Muratov, Phys. Rev. E **66**, 066108 (2002).
[7] C. Menotti, C. Trefzger, and M. Lewenstein, Phys. Rev. Lett. **98**, 235301 (2007).
[8] T. Garel and S. Doniach, Phys. Rev. B **26**, 325 (1982).
[9] P. G. de Gennes, Solid State Commun. **10**, 753 (1972); M. M. Fogler in *High Magnetic Fields. Applications in Condensed Matter Physics and Spectroscopy*, Lecture Notes in Physics Vol. 595, edited by C. Berthier, L. P. Levy, and G. Martinez (Springer, Berlin, 2001); B. Spivak and S. A. Kivelson, Phys. Rev. B **70**, 155114 (2004).
[10] A. Abanov, V. Kalatsky, V. L. Pokrovsky, and W. M. Saslow, Phys. Rev. B **51**, 1023 (1995).
[11] O. Portmann, A. Vaterlaus, and D. Pescia, Nature (London) **422**, 701 (2003).
[12] O. Portmann, A. Vaterlaus, and D. Pescia, Phys. Rev. Lett. **96**, 047212 (2006).
[13] See supplementary material at http://link.aps.org/supplemental/10.1103/PhysRevLett.104.077203 for an enlarged version of Fig. 1 and for details on the sample preparation, imaging, extraction of parameters, and the ground-state model.
[14] N. Saratz *et al.*, J. Phys. D **40**, 1268 (2007).
[15] J. Choi *et al.*, Phys. Rev. Lett. **98**, 207205 (2007).
[16] R. Plass, J. A. Last, N. C. Bartelt, and G. L. Kellogg, Nature (London) **412**, 875 (2001).
[17] A. B. Kashuba and V. L. Pokrovsky, Phys. Rev. B **48**, 10 335 (1993).
[18] A. Vindigni, N. Saratz, O. Portmann, D. Pescia, and P. Politi, Phys. Rev. B **77**, 092414 (2008).
[19] C. Kooy and U. Enz, Philips Res. Rep. **15**, 7 (1960); W. F. Druyvesteyn and J. W. F. Dorleijn, Philips Res. Rep. **26**, 11 (1971); J. A. Cape and G. W. Lehman, J. Appl. Phys. **42**, 5732 (1971).
[20] K.-O. Ng and D. Vanderbilt, Phys. Rev. B **52**, 2177 (1995).